Supplementary materials

Type-II $BiVO_4/Ni_3$(hexahydroxytriphenylene)$_2$ heterojunction photoanodes for effective photoelectrochemical reaction

Ji Won Yoon, Young-Moo Jo, Jong-Heun Lee*

Department of Materials Science and Engineering, Korea University, Seoul 02841, Republic of Korea

*Corresponding author. *E-mail address: jongheun@korea.ac.kr* (Jong-Heun Lee)

Material characterization

Morphological and structural characterizations of the $BiVO_4$ film and $BiVO_4/M_3(HHTP)_2$ (M = Ni, Co, Cu) were conducted using a field-emission scanning electron microscope (FE-SEM, SU-70) with an acceleration voltage of 5–10 kV and TEM (JEM-F200, JEOL Ltd, Japan). The phase and crystal structure of the $BiVO_4$ film and $BiVO_4/M_3(HHTP)_2$ (M = Ni, Co, Cu) were investigated via XRD (D/MAX-2500V/PC, Rigaku, Japan; Cu$K\alpha$, λ=1.5418 Å). The atomic compositions of the $BiVO_4/M_3(HHTP)_2$ (M = Ni, Co, Cu) were analyzed by XPS (X-TOOL, ULVAC-PHI, monochromatic Al-Kα = 1486.6 eV, Ag 3d5/2 < 0.48 eV). The reflection (R) and transmission (T) of the photoanodes were obtained using UV-vis spectroscopy (UV-vis, Jasco V-650). The band-bending diagrams of the $BiVO_4/M_3(HHTP)_2$ (M = Ni, Co, Cu) were investigated using ultraviolet photoelectron spectroscopy (UPS, AXIS-Nova; monochromatic He 1 = 21.2 eV, Ag $3d_{5/2}$ < 100 meV) and UV-vis spectroscopy.

PEC measurements

PEC water splitting was conducted in a 0.1 M Na_2SO_3 and 0.1 M Na_2SO_4 solution using a three-electrode electrochemical system (Ivium Technologies) equipped with $BiVO_4/M_3(HHTP)_2$ (M = Ni, Co, Cu) as the working electrode, a Pt mesh as the counter electrode, and Ag/AgCl/saturated NaCl as the reference electrode. A filter with the standard solar radiation of air mass (AM) 1.5 G was installed in the solar simulator, which was calibrated to 1 sun (100 mW/cm^2). The photoanodic performance was measured in the dark and under illumination using linear sweep voltammetry (LSV) at a scan rate of 20 mVs^{-1}. The measured potential vs. Ag/AgCl was converted to RHE using the Nernst equation:

$$E_{RHE=}E_{Ag/AgCl+}E^{0}_{Ag/AgCl+}0.059 * pH, \quad (1)$$

where E_{RHE} is the converted potential vs. RHE, $E_{Ag/AgCl}{}^{o}$ = 0.1976 V, and $E_{Ag/AgCl}$ is the measured potential vs. RHE and the Ag/AgCl reference. The IPCE was measured at an applied voltage of 1.23 V

vs. RHE under the irradiation source and monochromator (MonoRa150). The intensity at each wavelength was measured using a calibrated Si photodiode. The IPCE was calculated using the following equation:

$$IPCE\ (\%) = \frac{I_{ph}\left(mA\ cm^{-2}\right) \times 1239.8\ (V\ nm)}{P_{mono}\left(mW\ cm^{-2}\right)\ \times\ \lambda\ (nm)} \times 100 \quad , \tag{2}$$

where I_{ph} is the measured photocurrent density, λ is the wavelength of the incident light, and P_{mono} is the power intensity of the incident light at each wavelength. The IPCE considers three main factors: the light absorption efficiency (η_{abs}), charge separation efficiency (η_{sep}), and charge transfer efficiency (η_{trans}).

$$IPCE\ (\lambda) = \eta_{abs} \times \eta_{sep} \times \eta_{trans} \tag{3}$$

Electrochemical impedance spectroscopy (EIS) was performed in the frequency range of 100 kHz to 1 Hz with an applied voltage of 1.23 V vs. RHE. The EIS curves were fitted and analyzed to obtain the series resistance (R_s, Ω cm^2) and charge transfer resistance at the interface between the electrode and the electrolyte (R_{ct}, Ω cm^2). The product of the light-absorption and charge separation efficiencies ($\eta_{abs} \times \eta_{sep}$) and value of η_{trans} were obtained in 0.1 M Na_2SO_3 solution as a fast hole scavenger.

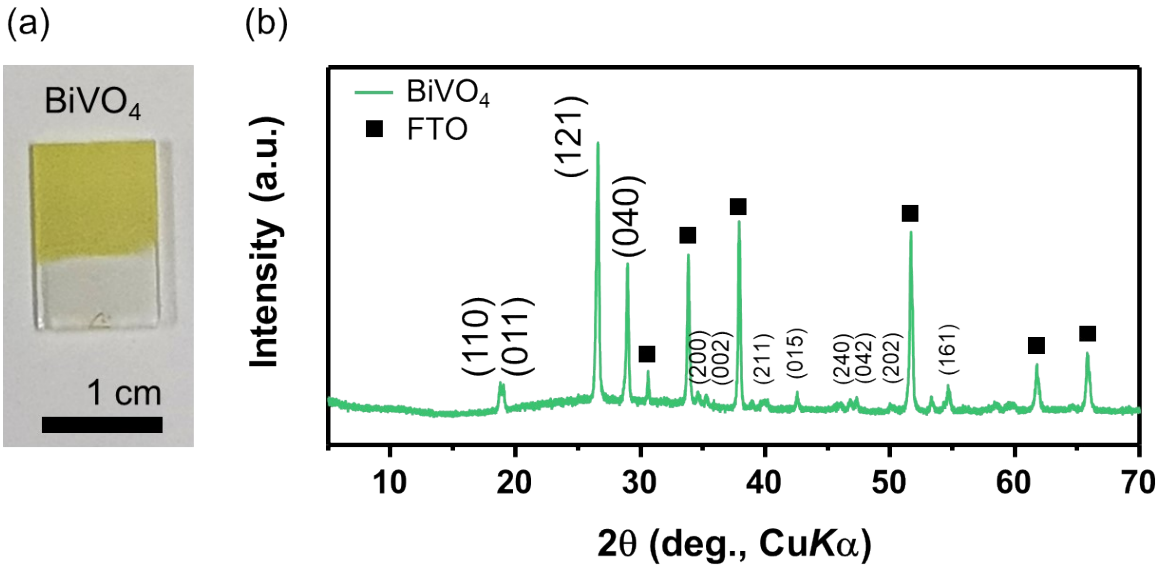

Fig. S1. (a) Photograph of $BiVO_4$/FTO/glass substrate. (b) XRD patterns of electrodeposited $BiVO_4$ on FTO/glass substrate.

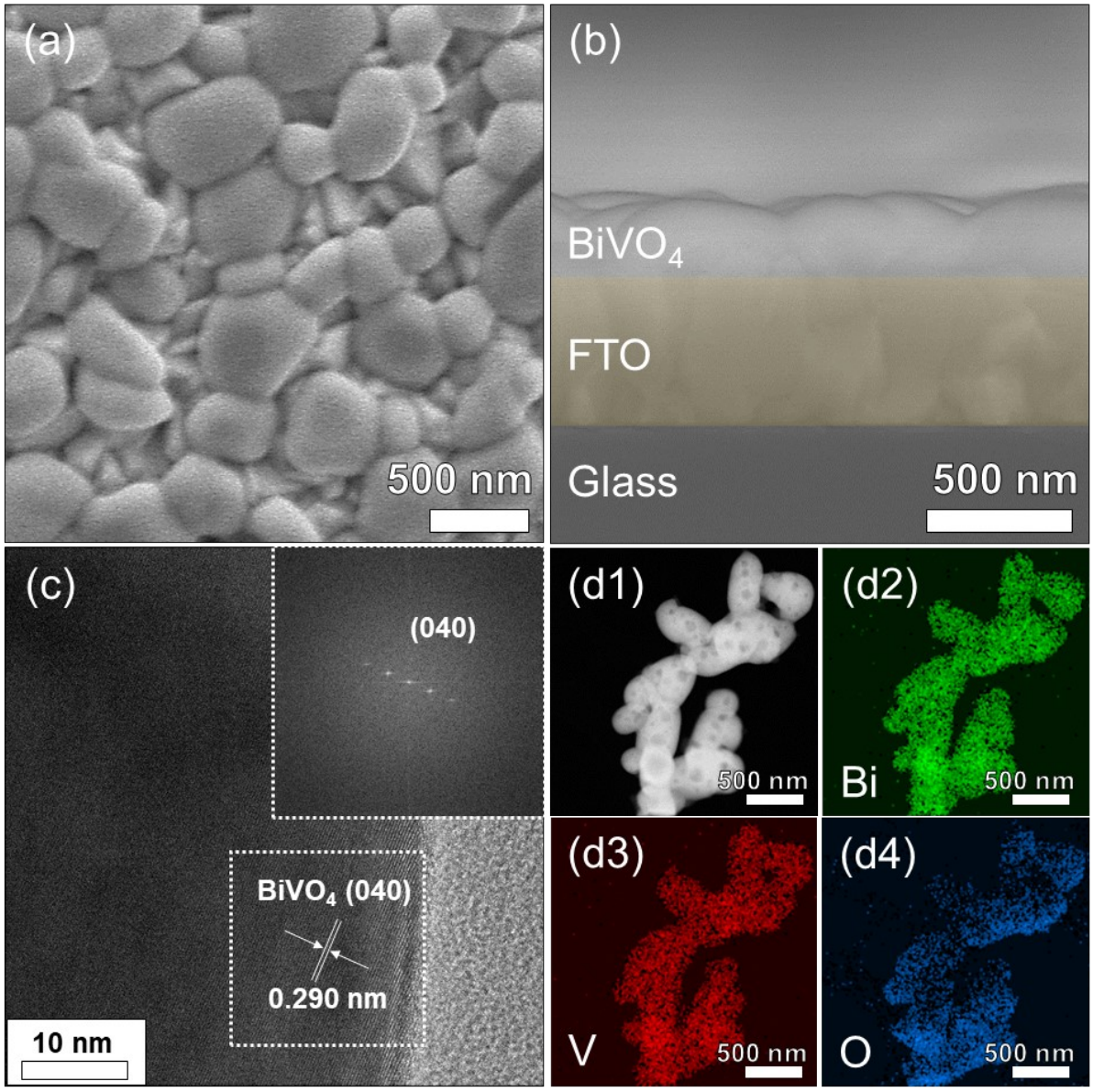

Fig. S2. (a) Top-view and (b) cross-sectional view SEM image of $BiVO_4$ thin film. (c) HR-TEM image of $BiVO_4$ (inset: SAED patterns). Elemental mappings of (d1) $BiVO_4$, (d2) Bi, (d3) V, and (d4) O.

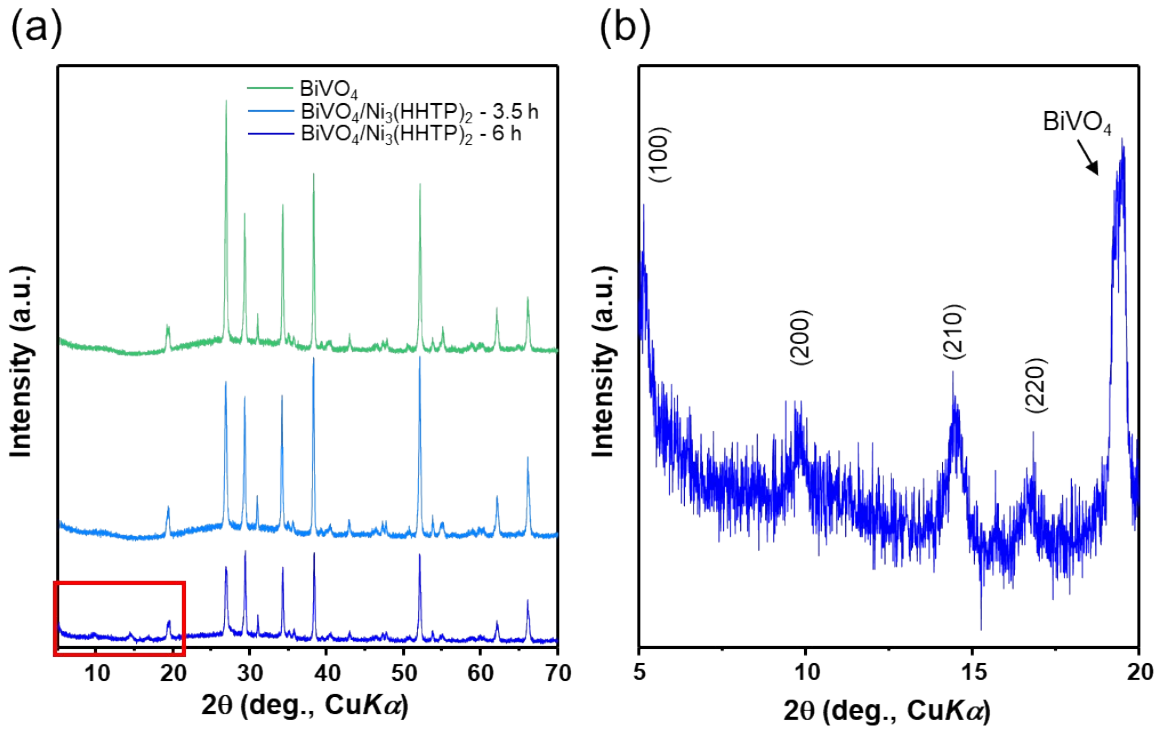

Fig. S3. (a) XRD patterns of $BiVO_4$ and $BiVO_4/Ni_3(HHTP)_2$ heterostructure (solvothermal 3.5 h and 6 h). (b) Close examination of XRD peaks at $2\theta=5\sim20^{o}$ of $BiVO_4/Ni_3(HHTP)_2$ (solvothermal 6 h).

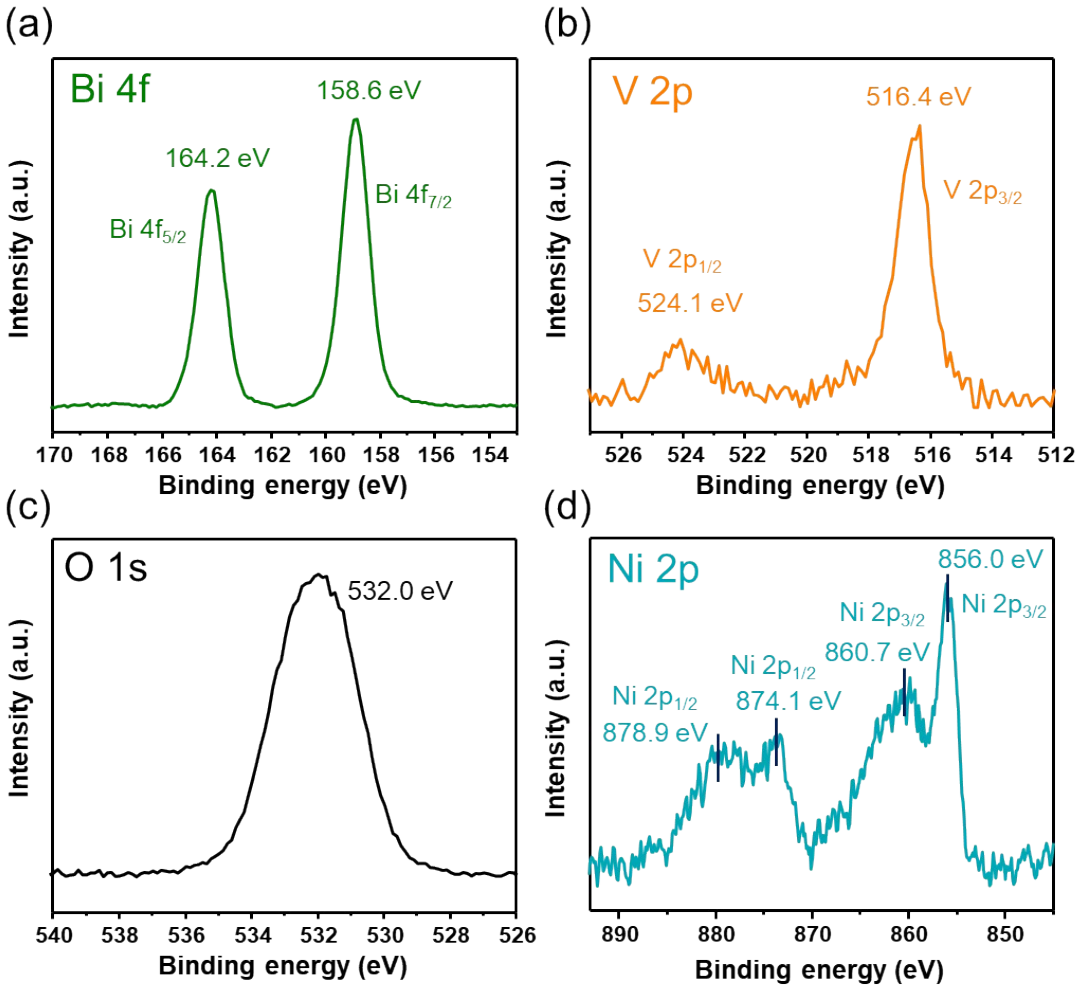

Fig. S4. XPS of (a) Bi 4f, (b) V 2p, (c) O 1s, and (d) Ni 2p in $BiVO_4/Ni_3(HHTP)_2$ heterostructure.

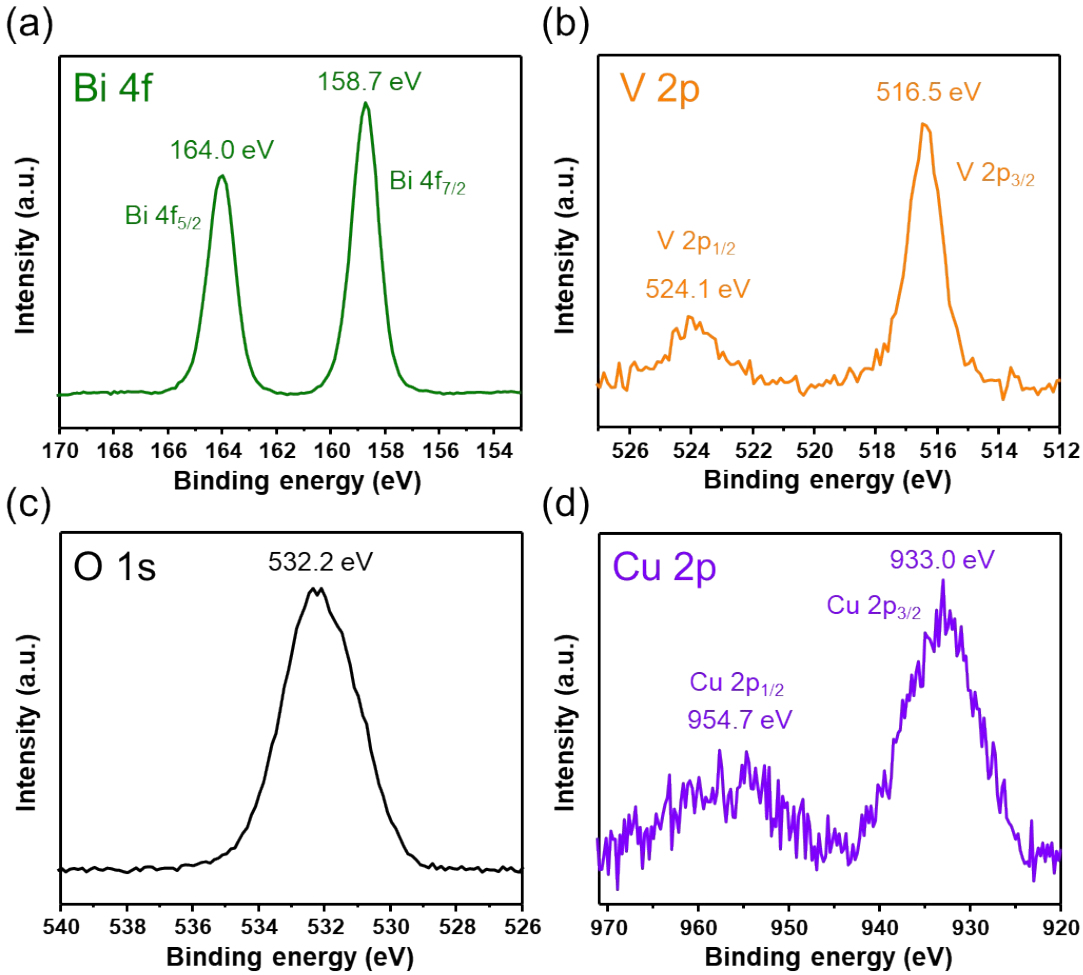

Fig. S5. XPS of (a) Bi 4f, (b) V 2p, (c) O 1s, and (d) Cu 2p in $BiVO_4/Cu_3(HHTP)_2$ heterostructure.

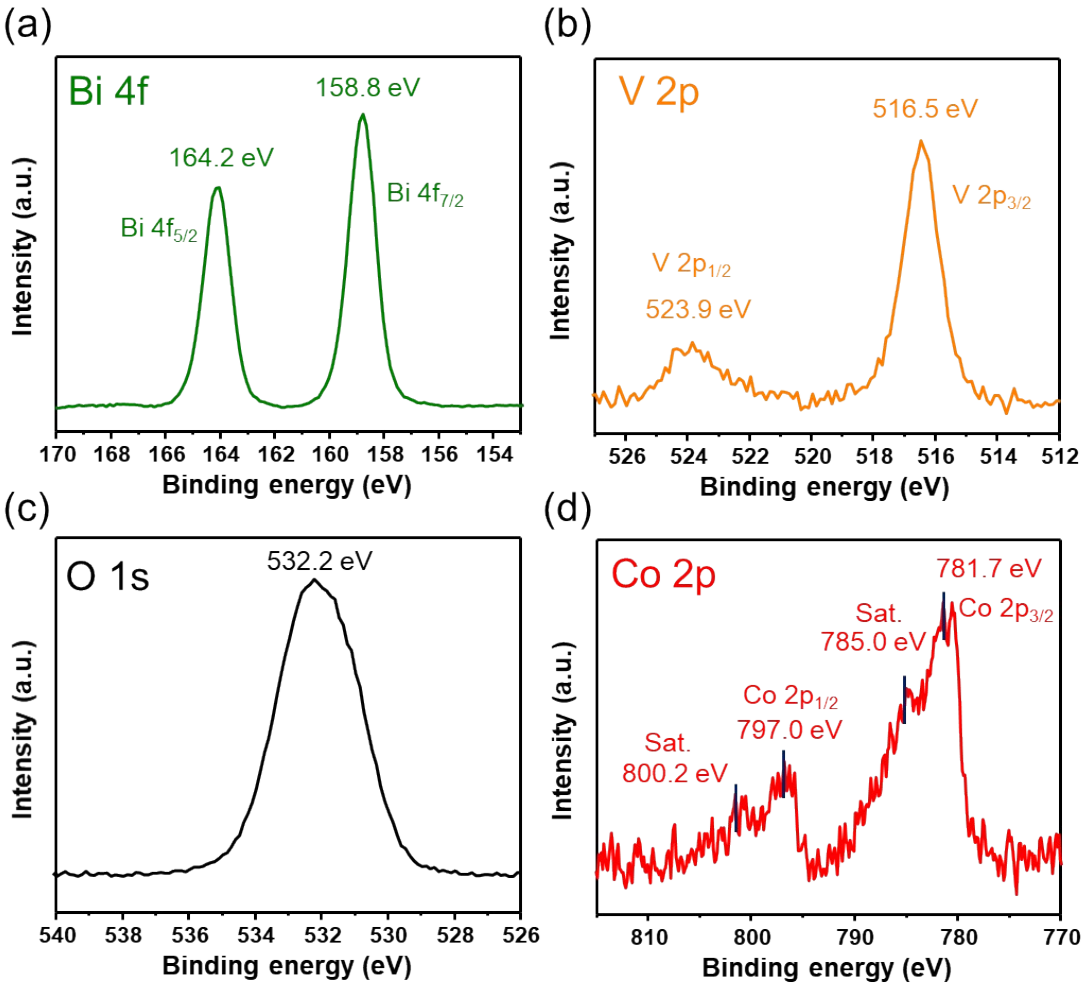

Fig. S6. XPS of (a) Bi 4f, (b) V 2p, (c) O 1s, and (d) Cu 2p in $BiVO_4/Co_3(HHTP)_2$ heterostructure.

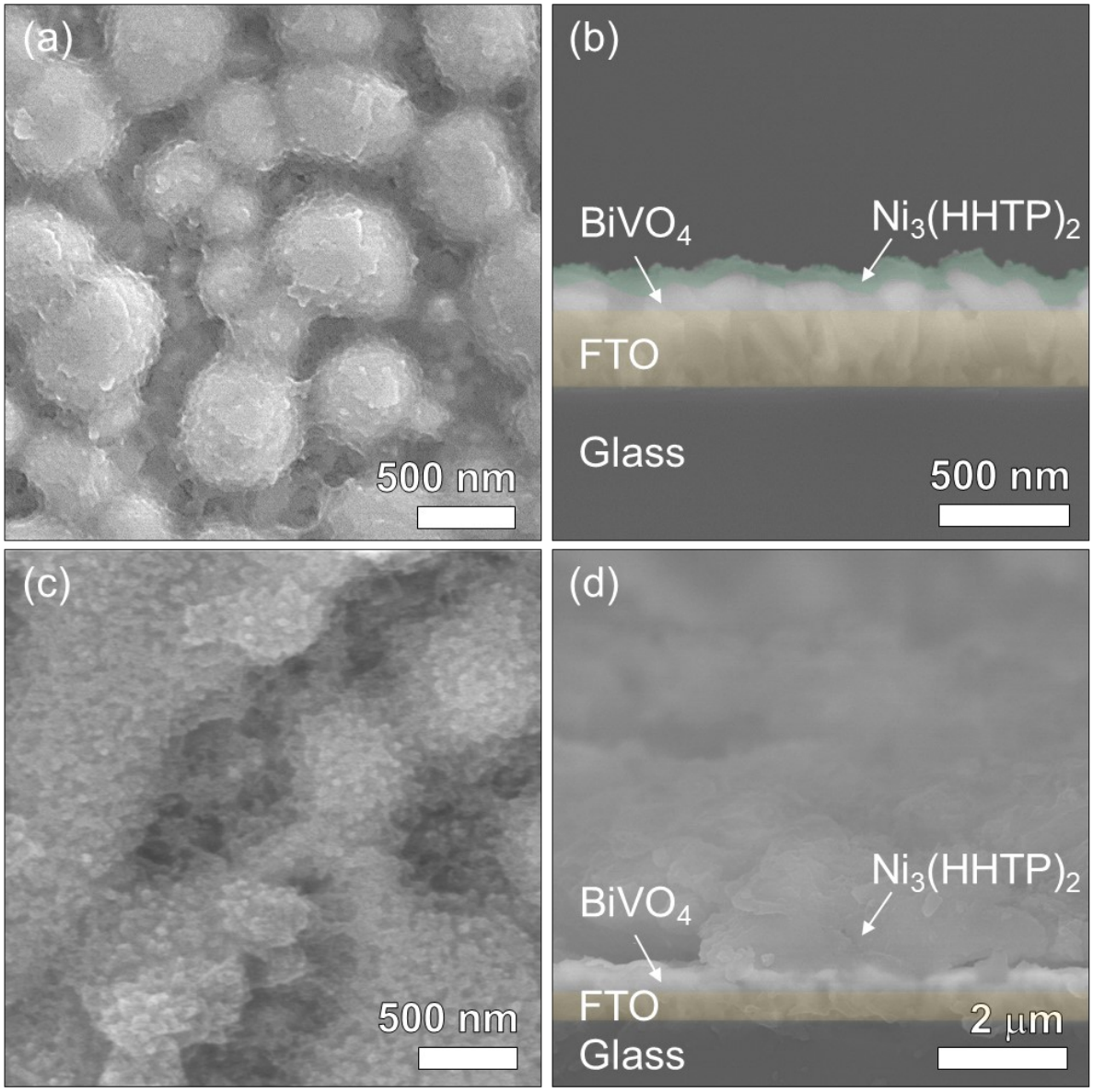

Fig. S7. (a) Top-view and (b) cross-sectional view SEM image of $BiVO_4/Ni_3(HHTP)_2$ heterostructure (solvothermal 1 h). (c) Top-view and (d) cross-sectional view SEM image of $BiVO_4/Ni_3(HHTP)_2$ heterostructure (solvothermal 6 h).

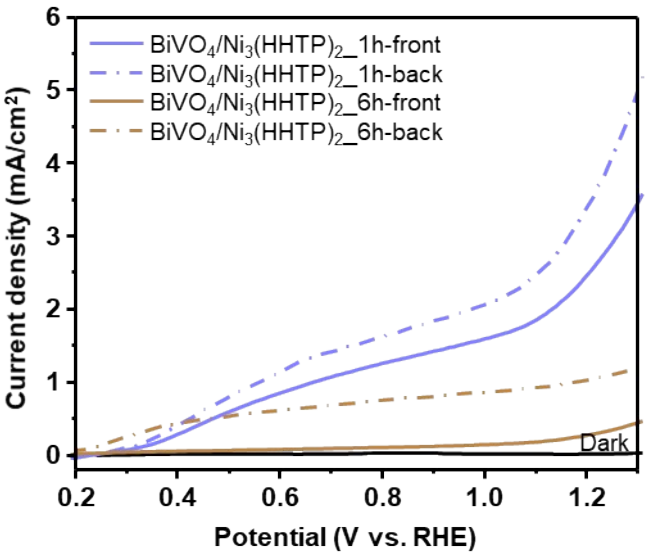

Fig. S8. *J-V* curves of $BiVO_4/Ni_3(HHTP)_2$ (solvothermal 1 h and 6 h) heterostructure in a 0.1 M Na_2SO_3.

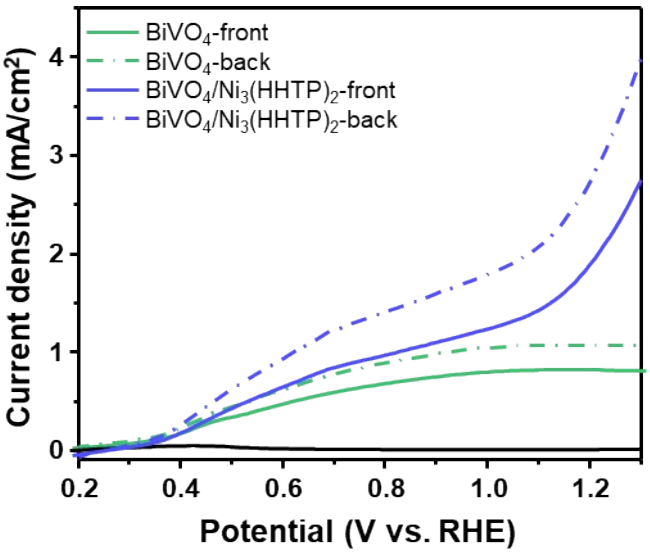

Fig. S9. (a) J-V curves of $BiVO_4$ and $BiVO_4/Ni_3(HHTP)_2$ in a 1 M Na_2SO_4 electrolyte (without hole scavenging Na_2SO_3). (b) Mott-Schottky plots of $BiVO_4$ and $BiVO_4/Ni_3(HHTP)_2$ at 100 Hz.

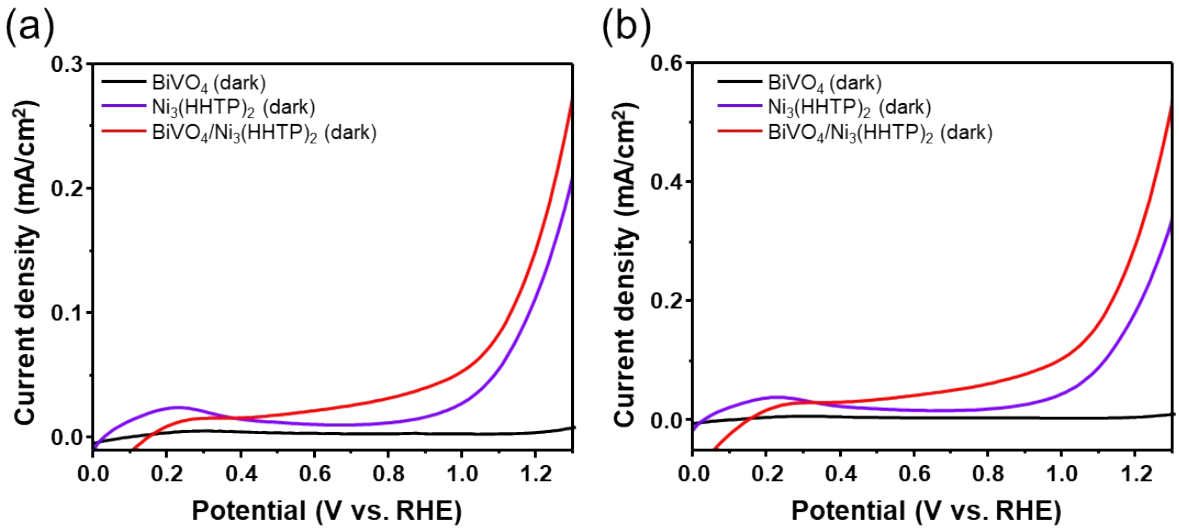

Fig. S10. (a) J-V curves of $BiVO_4$, $Ni_3(HHTP)_2$ and $BiVO_4/Ni_3(HHTP)_2$ in dark (0.1 M Na_2SO_4 electrolyte). (b) J-V curves of $BiVO_4$, $Ni_3(HHTP)_2$ and $BiVO_4/Ni_3(HHTP)_2$ in dark (0.1 M Na_2SO_3 electrolyte).

Table S1. Photocurrent densities of $BiVO_4$/MOF heterostructures at 1.23 V in the literatures and the present work. [S1-S7]

Photoanode	$J_{sulfite}$ @ 1.23 V (mA/cm^2)	J_{water} @ 1.23 V (mA/cm^2)	Ref
$BiVO_4/Ni_3(HHTP)_2$	4.66	3.10	This work
$BiVO_4$/Bi-MOF	3.21	2.35	[S1]
Fe-doped $BiVO_4$/MIL-53(Fe)	-	1.15	[S2]
$BiVO_4$/MIL-101(Fe)	-	2.59	[S3]
$BiVO_4$/Co-Ni-MOF	-	3.20	[S4]
$BiVO_4$@Co-MIm		3.16	[S5]
$BiVO_4$/Co-MOF	-	3.10	[S6]
Fe/W-doped $BiVO_4$/MIL-100(Fe)	-	2.76	[S7]

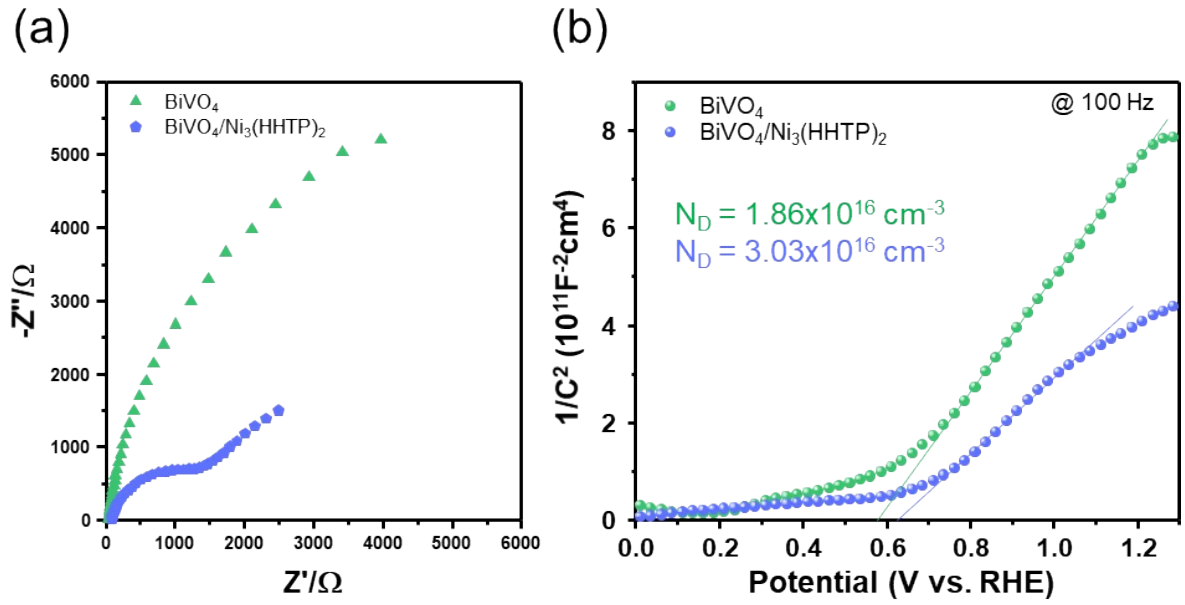

Fig. S11. (a) EIS analysis for $BiVO_4$ and $BiVO_4/Ni_3(HHTP)_2$ at 0V in dark. (b) Mott-Schottky plots of $BiVO_4$ and $BiVO_4/Ni_3(HHTP)_2$ at 100 Hz.

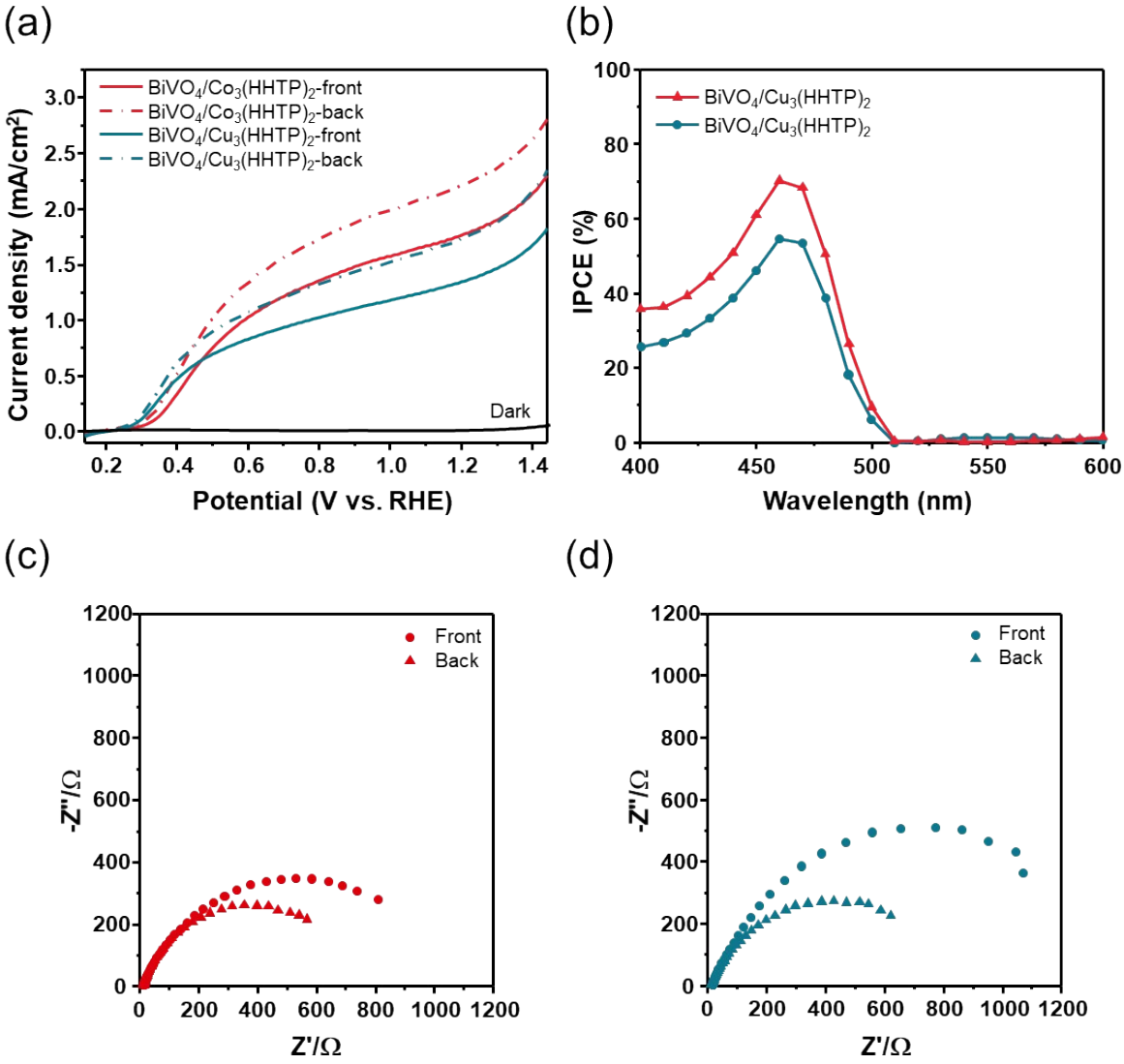

Fig. S12. (a) J-V curves of $BiVO_4/Co_3(HHTP)_2$ and $BiVO_4/Cu_3(HHTP)_2$ (front and back illumination) in a 0.1 M Na_2SO_3 electrolyte. (b) IPCE of $BiVO_4/Co_3(HHTP)_2$ and $BiVO_4/Cu_3(HHTP)_2$. EIS analysis of (c) $BiVO_4/Co_3(HHTP)_2$ and (d) $BiVO_4/Cu_3(HHTP)_2$ (front and back illumination).

Table S2. Fitted charge transfer resistance.

Photoanode	R_s ($W \cdot cm^2$)	R_{ct} ($W \cdot cm^2$)
$BiVO_4/Co_3(HHTP)_2$ (front)	11.9	1124.8
$BiVO_4/Co_3(HHTP)_2$ (back)	9.8	743.6
$BiVO_4/Cu_3(HHTP)_2$ (front)	10.5	1408.3
$BiVO_4/Cu_3(HHTP)_2$ (back)	11.4	803.2

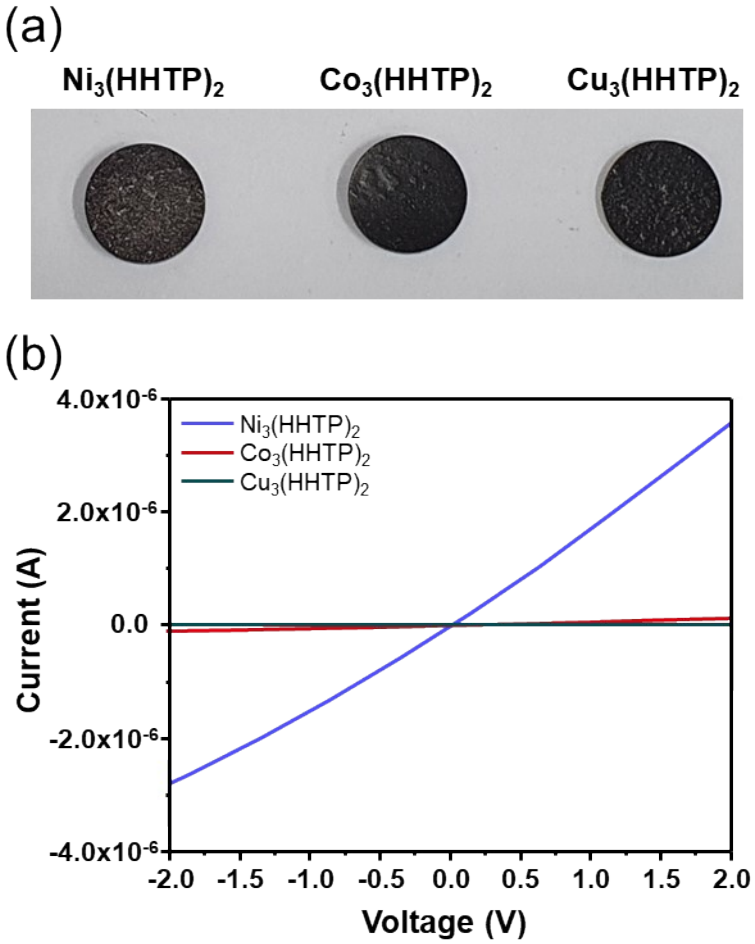

Fig. S13. (a) Pellets of $Ni_3(HHTP)_2$,$Co_3(HHTP)_2$, and $Cu_3(HHTP)_2$. (b) I-V curves of $Ni_3(HHTP)_2$,$Co_3(HHTP)_2$, and $Cu_3(HHTP)_2$ pellets. Electrical measurements of HHTP-based MOFs are performed using two-electrode in air at a constant temperature of 297 K and in the absence of light. The electrical conductivity is calculated to be $\sigma=4.45\times10^{-6}$ S cm^{-1}, $\sigma=1.59\times10^{-7}$ S cm^{-1}, $\sigma=4.29\text{x}10^{-8}$ S cm^{-1} for $Ni_3(HHTP)_2$,$Co_3(HHTP)_2$, and $Cu_3(HHTP)_2$, respectively. ($\sigma = L/(R\times\pi(d/2)^2$), L = 2.0 mm, d = 3.0 mm, $R_{Ni3(HHTP)2}= 6.35\times10^5\ \Omega$, $R_{Co3(HHTP)2}= 1.78\times10^7\ \Omega$, $R_{Cu3(HHTP)2}= 6.59\times10^7\ \Omega$)

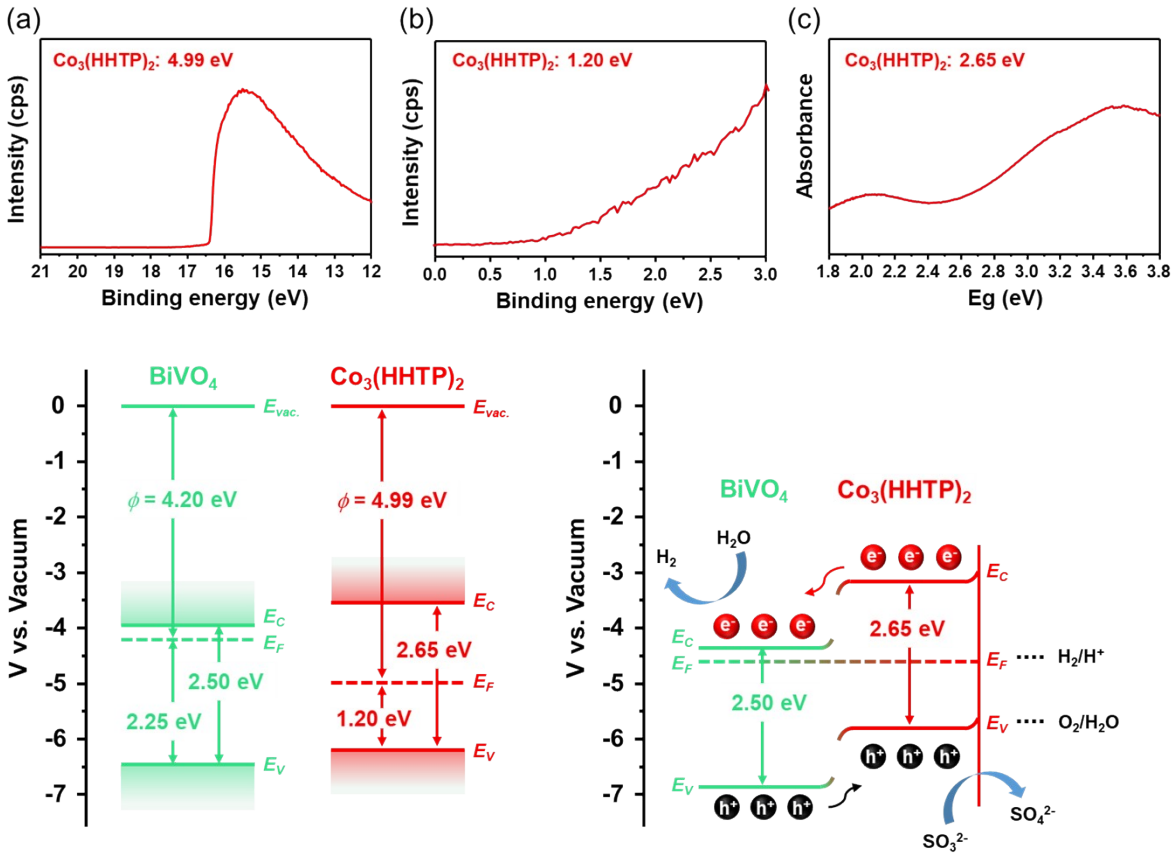

Fig. S14. UPS spectra of $BiVO_4$ and $BiVO_4/Co_3(HHTP)_2$ for obtaining (a) work function (*f*) and valence band maximum. (c) UV-vis spectra of $BiVO_4$ and $BiVO_4/Co_3(HHTP)_2$. Schematic energy band diagram of $BiVO_4$ and $BiVO_4/Co_3(HHTP)_2$ (d) before contact and (e) after contact.

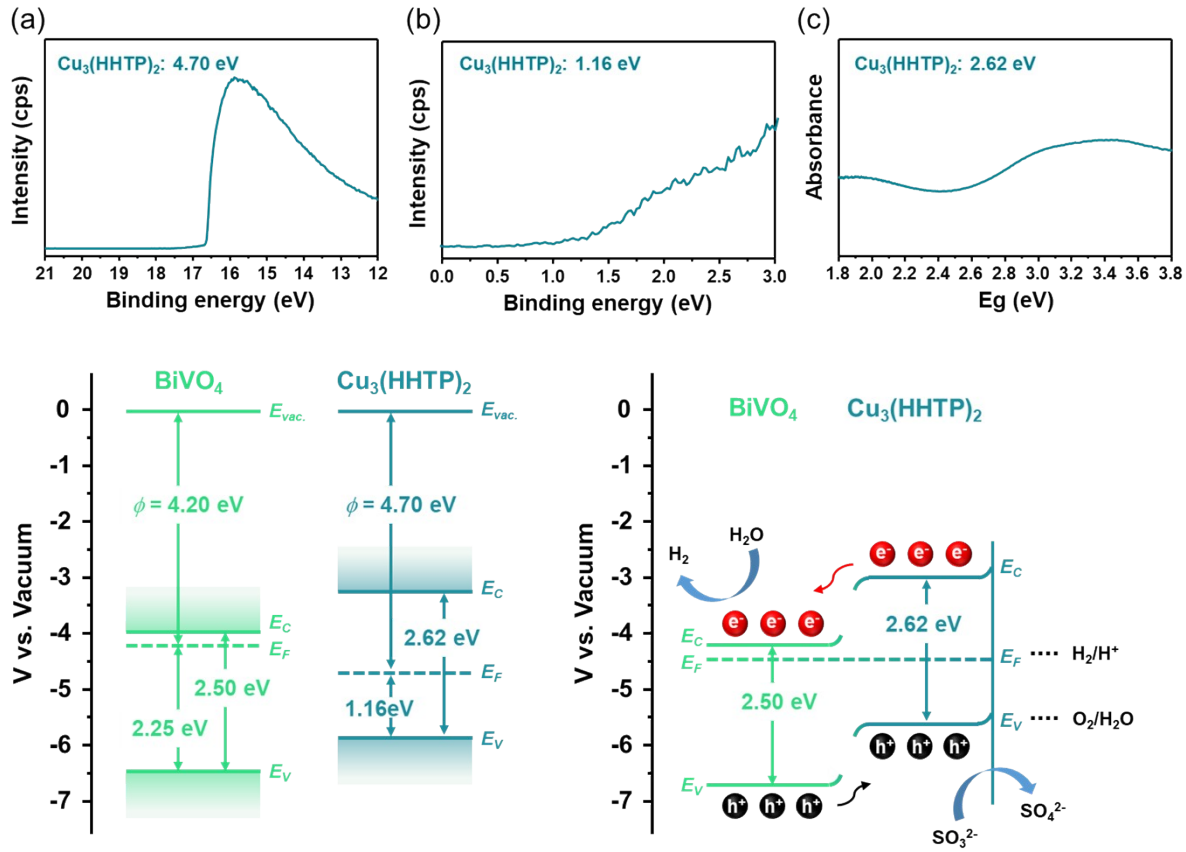

Fig. S15. UPS spectra of $BiVO_4$ and $BiVO_4/Cu_3(HHTP)_2$ for obtaining (a) work function (*f*) and valence band maximum. (c) UV-vis spectra of $BiVO_4$ and $BiVO_4/Cu_3(HHTP)_2$. Schematic energy band diagram of $BiVO_4$ and $BiVO_4/Cu_3(HHTP)_2$ (d) before contact and (e) after contact.

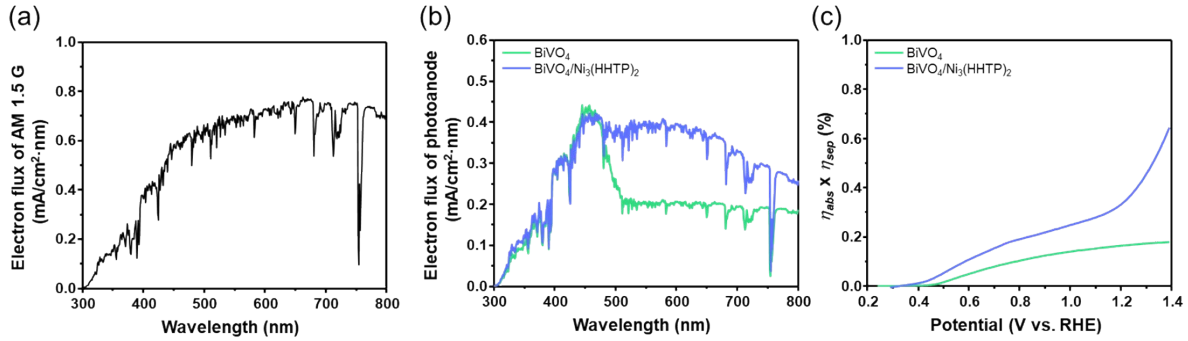

Fig. S16. (a) Electron flux of AM 1.5 G solar spectrum. (b) Electron flux of $BiVO_4$ and $BiVO_4/Ni_3(HHTP)_2$. The electron flux of the photoanode is the product of AM 1.5 G electron flux and LHE (%). (c) η_{abs} x η_{sep} of $BiVO_4$ and $BiVO_4/Ni_3(HHTP)_2$.

Table S3. Light absorption wavelength, J_{max}, J_{abs}, and η_{abs} of $BiVO_4$ and $BiVO_4/Ni_3(HHTP)_2$.

Photoanode	**Light absorption wavelength (nm)**	J_{max} **(mA/cm^2)**	J_{abs} **(mA/cm^2)**	η_{abs} **(%)**
$BiVO_4$	496	6.44	4.42	68.6
$BiVO_4/Ni_3(HHTP)_2$	504	6.95	4.89	70.4

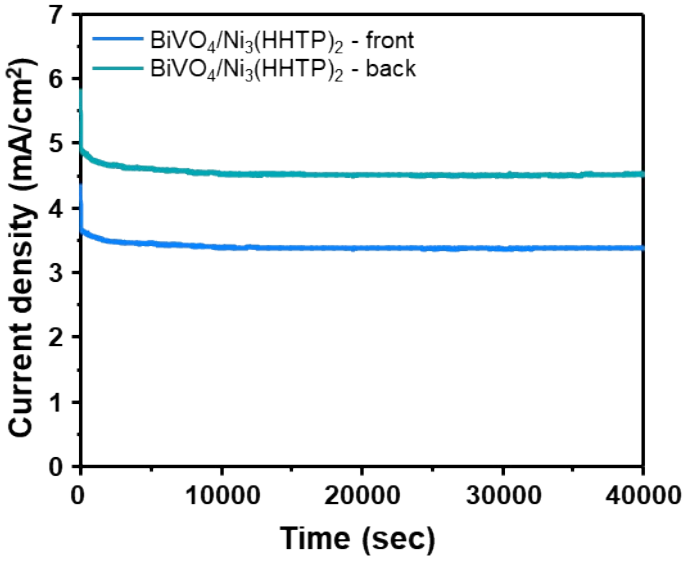

Fig. S17. The chronopotentiometry curve of $BiVO_4/Ni_3(HHTP)_2$ in a 0.1 M Na_2SO_3 electrolyte at 1.23 V vs. RHE under front and back illumination.

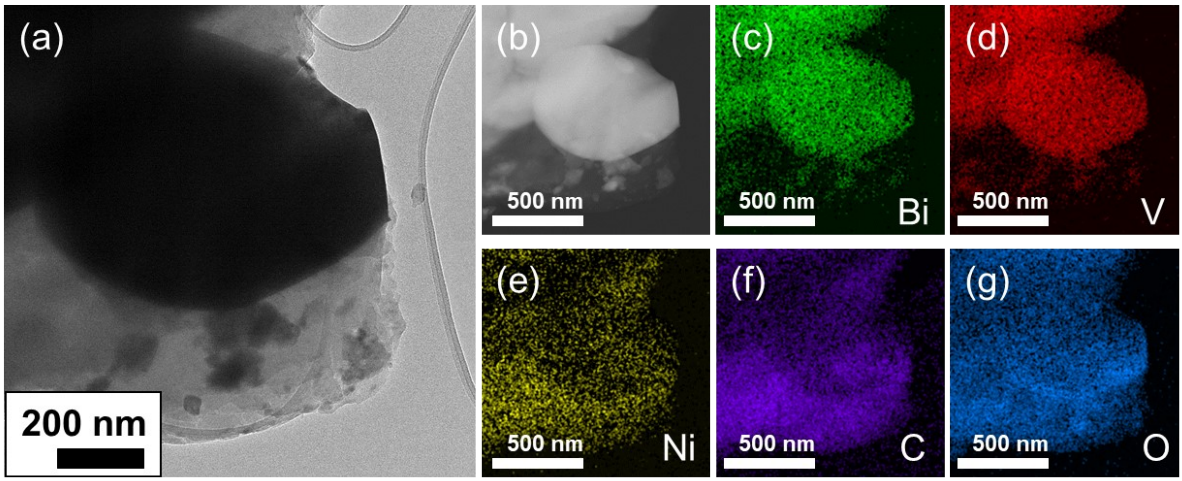

Fig. S18. (a) TEM image and (b-g) elemental mappings of $BiVO_4/Ni_3(HHTP)_2$ heterostructure after photoelectrochemical reaction.

Reference

[S1] S. Kim, T.A.D. Pena, S. Seo, H. Choi, J. Park, J.H. Lee, J. Woo, C.H. Choi, S. Lee, *Appl. Surf. Sci.*, 2021, **563**, 150357.
[S2] G.X. Liu, Y.P. Li, Y. Xiao, D.M. Jia, C.H. Li, J.J. Zheng, X.W. Liu, *Catal. Lett.*, 2019, **149**, 870-875.
[S3] C.H. Liu, H. Luo, Y. Xu, Z.H. Zhang, Q. Liang, W.C. Wang, Z.D. Chen, *Chem. Eng. J.*, 2020, **384**, 123333.
[S4] S.Q. Zhou, K.Y. Chen, J.W. Huang, L. Wang, M.Y. Zhang, B. Bai, H. Liu, Q.Z. Wang, *Appl. Catal. B*, 2020, **266**, 118513.
[S5] S.Q. Zhou, P.F. Yue, J.W. Huang, L. Wang, H.D. She, Q.Z. Wang, *Chem. Eng. J.*, 2019, **371**, 885-892.
[S6] W. Zhang, R. Li, X. Zhao, Z. Chen, A.W.K. Law, K. Zhou, *Chemsuschem*, 2018, **11**, 2710-2716.
[S7] Z.B. Jiao, J.J. Zheng, C.C. Feng, Z.L. Wang, X.S. Wang, G.X. Lu, Y.P. Bi, *Chemsuschem*, 2016, **9**, 2824-2831.